Polymer-assisted modification of metal-organic framework MIL-96 (Al): influence on particle size, crystal morphology and perfluorooctanoic acid (PFOA) removal

Luqman Hakim Mohd Azmi [†,§,‡], *Daryl Williams* [‡], *Bradley P. Ladewig* [†,∥,*]

[†]Barrer Centre, Department of Chemical Engineering, Imperial College London, South Kensington Campus, SW7 2AZ, London, United Kingdom.

[§]Grantham Institute – Climate Change and the Environment, Imperial College London, South Kensington Campus, SW7 2AZ, London, United Kingdom.

[‡]Surfaces and Particle Engineering Laboratory (SPEL), Department of Chemical Engineering, Imperial College London, South Kensington Campus, SW7 2AZ, London, United Kingdom.

[∥] Institute for Micro Process Engineering (IMVT), Karlsruhe Institute of Technology, Hermann-von-Helmholtz-Platz 1, 76344 Eggenstein-Leopoldshafen, Germany.

[*] Corresponding author's email: bradley.ladewigkit.edu

Keywords. Polymer, particle size, crystal morphology, metal-organic frameworks, perfluorooctanoic acid, adsorption.

Abstract

A new synthesis method was developed to prepare an aluminum-based metal organic framework (MIL-96) with a larger particle size and variable crystal aspect ratio. A low cost and water-soluble polymer, hydrolyzed polyacrylamide (HPAM), was added in varying quantities into the synthesis reaction to achieve >200% particle size enlargement with controlled crystal morphology. The modified adsorbent, MIL-96-RHPAM2, was systematically characterized by SEM, XRD, FTIR, BET and TGA-MS. Using activated carbon (AC) as a reference adsorbent, the effectiveness of MIL-96-RHPAM2 for perfluorooctanoic acid (PFOA) removal from water was examined. The study confirms stable morphology of hydrated MIL-96-RHPAM2 particles as well as a superior PFOA adsorption capacity (340 mg/g) despite its lower surface area, relative to standard MIL-96. MIL-96-RHPAM2 suffers from slow adsorption kinetics as the modification significantly blocks pore access. The strong adsorption of PFOA by MIL-96-RHPAM2 was associated with the formation of electrostatic bonds between the anionic carboxylate of PFOA and the amine functionality present in the HPAM backbone. Thus, the strongly held PFOA molecules in the pores of MIL-96-RHPAM2 were not easily desorbed even after elution with a high ionic strength solvent (500 mM NaCl). Nevertheless, this simple HPAM addition strategy can still chart promising pathways to impart judicious control over adsorbent particle size and crystal shape while the introduction of amine functionality onto the surface chemistry is simultaneously useful for enhanced PFOA removal from contaminated aqueous systems.

1. Introduction

Adequate, clean and safe water supply is indispensable to healthy wellbeing of humans and living organisms.[1] Unfortunately, our surface and ground waters continue being polluted by industrial waste streams containing toxic and persistent chemicals including perfluorinated compounds (PFCs). PFCs have recently received much attention because they are ubiquitous contaminants in water, wildlife, and humans. The most commonly found PFCs in surface waters are perfluorooctanoic acid (PFOA) and perfluorooctane sulfonate (PFOS).[2] Surprisingly, thus far, there is no mutually agreed international drinking water standard for PFOA and PFOS, but the United States Environmental Protection Agency have recommended a strict combined concentration limit of 70 ng/L.[3] Recent analysis of global water samples even revealed concentrations exceeding the provisional threshold.[4–9]

Although most fluorochemical manufacturers have ceased their production of PFOA and PFOS in the early 2000s, this measure does not address the legacy pollution caused by these compounds. The ubiquitous presence and long-range mobility of PFCs is attributed to the high chemical stability of their C-F bonds (bond dissociation energy, $D^{\circ}_{298\ K}$ = 485 kJ/mol),[10] rendering them suitable as ingredients to make fluoropolymers,[11] fire-fighting foams,[3] and stain-repellent products.[10] Typical contamination hot spots then include the vicinity of industrial areas, military training sites, airports and wastewater treatment plants.[12] Moreover, exposures to PFCs adversely affect body immunity,[13] neurological functions,[14] reproductive systems[15] as well as giving strong

correlations to coronary heart disease[16] and cancer[17] among many others. As a result, there is an urgent need to investigate efficient materials for PFCs remediation from contaminated water.

Of the treatments available for PFCs removal from water,[18] adsorption is extensively used given its simplicity, relatively lower cost and high selectivity.[19] Studied adsorbents range from activated carbon (AC),[20,21] minerals,[22,23] magnetic nanoparticles,[24] polymers,[25] resins,[26] functionalized cellulose[27] and metal-organic frameworks (MOFs).[28–32] However, except for MOFs, most adsorbents only exhibit between low and moderate PFOA uptake compared to the industrial standard of AC (>90% removal, 3M Company, USA).[33]

MOFs refer to a novel class of porous materials made from organic bridging linkers and metal atoms. Distinguishing MOF features include their high surface areas, ready structure tunability and reusability via simple washing procedures which means that these materials are seen as a promising future substitute for AC.[34] Further to that, in commercial water purification processes, adsorbents are generally deployed into a packed bed for continuous filtration. Fluids flowing through some packed beds may at times result in high pressure drops. This directly increases the energy requirement to pump the fluid through the bed and decreases the operational lifetime of the pumps, impacting on the economics of the process.[35] Although various factors are involved in optimal bed design, lowering the pressure drop can be easily achieved by increasing the adsorbent particle size.[36] Larger particles also facilitate easier recovery in between the washing cycles.

Size and crystal morphology of MOFs can be precisely controlled via the presence of additives[37] such as initiation solvents,[38,39] coordination modulators or capping agents,[40–42] surfactants,[43] and hard templates[44] or through synthetic techniques using pyrolysis,[45] ultrasound[46] and microreactor.[47] Some complexities regarding the respective methods are usage of harmful organic solvents, use of acidic or basic modulators that increase risk of safety hazards and difficulty in isolating the hard templates after preparation. Whilst these three MOF synthetic techniques can only be carried out with specialized instrument, a common limitation of these approaches is the formation of predominantly nanoparticle products. The work reported here uses a surfactant-assisted method which serves as a multifaceted approach; functioning as a nanoreactor, a capping agent as well as a molecular template.[37]

The current study highlights a new one-pot surfactant-based synthesis method to control particle size and morphology of MOF crystals by utilizing a synthetic polymer, hydrolyzed polyacrylamide (HPAM). HPAM is a low cost and water-soluble polymer widely used for enhanced oil recovery in petroleum drilling processes, as well as being used as a flocculant for wastewater treatment[48] where its benign effects on water quality are noted.[49] Finally, a non-toxic and hydrothermally stable aluminum-based MOF, MIL-96 (Al) was chosen to be tested for liquid phase adsorption of PFOA. Given the positive surface charge for MIL-96,[50] HPAM must be anionic to initiate particle aggregation. In addition, PFOA adsorption performance by the modified material was benchmarked with a commercial AC to understand the interaction mechanisms better.

2. Experimental Section

Chemicals. Polyacrylamide (PAM) (FLOPAM FA 920 SH, non-ionic) and partially hydrolyzed polyacrylamide (HPAM) (FLOPAAM FP3630S, anionic, 25–35 mol% hydrolyzed) were supplied by SNF Floeger (France). Polyacrylic acid sodium salt (Na-PAA, average Mw~2100), 2,2,2-trifluoroethanol (TFE, 99.5%), perfluorooctanoic acid (PFOA, 95%), ammonium acetate (AA, 99.0%), trimesic acid (TMA, 95%), sodium chloride (NaCl, 99%) were purchased from Sigma Aldrich. Deuterium oxide (D_2O, 99.90%) and aluminum nitrate nonahydrate ($Al(NO_3)3.9H_2O$, 98%) were purchased from Fluorochem and Alfa Aesar respectively. All other chemicals and solvents were reagent grade and used without further purification. Ultrapure water (H_2O) used throughout the study was obtained from PureLab Chorus ELGA unit. Granular activated carbon (AC) F400 was procured from Chemviron Carbon as a high-grade, steam-activated bituminous coal.

^{19}F NMR analysis. Concentration for the internal standard (TFE) solution was set to 2.3 mM by transferring 0.42 mL TFE into 1 L H_2O. The NMR analyte consists of 0.25 mL D_2O, 0.25 mL filtrate and 0.2 mL TFE. Quantification was performed according to the literature.[28] Integrated area under the characteristic peaks of the terminal CF_3 groups for PFOA (-80 ppm) was compared relative to the TFE peaks (-76 ppm). Residual PFOA concentration after adsorption was calculated from the linear calibration equation obtained.

Adsorption. Prior to adsorption, the adsorbents were activated overnight at 120 °C under vacuum. All sorption experiments were conducted at room temperature. A PFOA stock solution

(1000 mg/L) was prepared using ultrapure H_2O. Adsorbent (20 mg) was added with a 20 mL PFOA solution into a screw cap vial, stirred for 72 hours and then, the solution was filtered. The filtrate was collected for NMR analysis while the filtered solids were reused for desorption. The experiments were performed in duplicate and the average values are reported.

Desorption. Based on the result from the desorption solvent screening, the solvent composition was adjusted to get a mixed methanol/ water (3:1, v/v) stabilized with 10 mM AA buffer solution. To study the influence of NaCl on the desorption efficiency, four desorption solvents were prepared with varying NaCl concentrations namely: RS1 (no salt), RS2 (10 mM NaCl), RS3 (50 mM NaCl) and RS4 (500 mM NaCl). After 72 hours of adsorption, the adsorbent was recovered by filtration and placed respectively in 20 mL desorption solvent containing the above NaCl concentrations to be continuously stirred for another 72 hours at room temperature. Sample preparation for NMR analysis followed the steps mentioned previously.

Hydrothermal Synthesis of MOF. MIL-96 was synthesized according to the original method described previously[51] whereas the protocol for polymer addition was adapted from another study.[52] A typical hydrothermal synthesis solution contains $Al(NO_3)_3.9H_2O$ (1.3 g, 3.5 mmol), TMA (0.1 g, 0.5 mmol) and H_2O (5 mL, 278 mmol) in a 23 ml Teflon liner. Firstly, to induce particle aggregation, HPAM solution (1000 mg/L) was poured into the reacting solution containing only the dissolved linker in H_2O. The solution was later sonicated for 15 minutes prior to adding the metal precursor. The ratio between the volume of polymer solutions added to the volume of water (R) is defined below. The mixture was heated to 210 °C for 24 hours. After cooling to ambient conditions, the resulting solid product was recovered via filtration and consequently washed with

copious amount of H_2O. The washed residue was dried at 120 °C *in vacuo* overnight. Similar steps were implemented when using other polymer solutions (PAM and Na-PAA). Chemical structures for all the polymers are illustrated in Figure S1 of the Supporting Information (SI).

$$R = \frac{Volume\ of\ polymer\ (mL)}{Volume\ of\ water\ used\ as\ solvent\ in\ the\ reaction\ (mL)}$$

3. Results and Discussion

SEM. For MIL-96, HPAM is proven effective in changing the MOF particle morphology as observed in Figure 1–3. Generally, starting from the normally reported small hexagonal bipyramidal shaped (HB) crystals,[53] higher HPAM concentrations facilitate incremental increases in the aspect ratio (length : diameter), transitioning from hexagonal spindles (HS) to elongated hexagonal rods (HR), particularly when 20 mL HPAM was used (MIL-96-RHPAM2). Upon closer inspection from out-of-plane PXRD measurements, the apparent HS morphology was revealed to be a hybrid form of two elongated hexagonal pyramids seamlessly connected at the long axis.[54]

It was reported that the hydrothermal synthesis conditions for MIL-96 must be strictly controlled given the possibility of forming two larger pore Al trimesates, MIL-100 and MIL-110, in the same reaction system despite all having distinct crystal structures. MIL-100 is the kinetically stable product which forms at short reaction times and low pH condition whereas the thermodynamically favored MIL-96 can be obtained after longer reaction times. MIL-110, on the other hand, crystallizes in a much more acidic or basic medium.[55] Their corresponding crystal morphologies have also been solved with MIL-96, MIL-100 and MIL-110 presenting a flat hexagonal, an octahedral and a hexagonal needle-like habits respectively.[56] Therefore, the influence of HPAM on the crystal morphology agrees well with the stability order of these phases; MIL-96 > MIL-110 > MIL-100.

The addition of HPAM seems to play multiple roles in the crystal elongation phenomenon, firstly as a competing modulator. Since the pK_a value for HPAM (4.5)[57] is similar to that of TMA (pK_{a1} =

3.51, pK_{a2} = 3.89, pK_{a3} = 4.70), there will be competition with the linker to form coordination bonds with available Al. As a result, nucleation rate slows down and permits slow growth of large MOF crystals.[58] Secondly, the amine ($-NH_2$) groups in both HPAM and PAM increase the basicity of the reacting solution, providing ideal conditions for the formation of MIL-110 ascribed by the existence of HR crystals. HPAM is a copolymer composed of PAM and Na-PAA. To identify the dominant functional groups responsible to the formation of HR, MIL-96 was synthesized using equivalent concentrations of PAM and Na-PAA separately. Before the reaction, the solutions were very acidic upon addition of PAM (pH = 2), Na-PAA (pH = 2.4) and HPAM (pH =2.2). Such acidic environment increases the likelihood of $-NH_2$ groups protonating to form primary ammonium ions ($-NH_3^+$) in preference to the ionization of the -COOH groups on the TMA due to higher pK_a values. It is therefore expected to see the $-NH_2$ groups contained in HPAM and PAM to govern the crystal elongation mechanism, transforming the HB shape into the HR habit more so than using Na-PAA.

Following the addition of 20 mL Na-PAA, it is unclear what drives the formation of new hexagonal lumps (HL) with some truncated and larger in dimension among the HR. What might have happened is, from the instant of mixing Na-PAA in water, the dissociated Na^+ cations may end up competing with the Al^{3+} species to form bonds with the linker, causing deceleration in the crystal growth and altering the original template. Another factor that may have undermined Na-PAA's influence is due to its low molecular weight (~2100 g/mol). By substituting higher molecular weight PAA for the synthesis, its influence toward crystal elongation may be amplified. Finally, the successes in morphological change shown in the MIL-96 samples can be attributed to the solubility of the linker (TMA) in water. Simultaneous dissolution of both TMA and HPAM

during the pre-mixing stage facilitates smooth integration of the latter species into the reacting solution, which subsequently changes the MOF crystal morphology. On a side note, identical experiments were performed involving similar modification of another MOF. Readers are referred to Figures S2 – S4 in the SI for further information. Scheme 1 provides an overview of the effects of HPAM addition in relation to MIL-96 crystal shape changes.

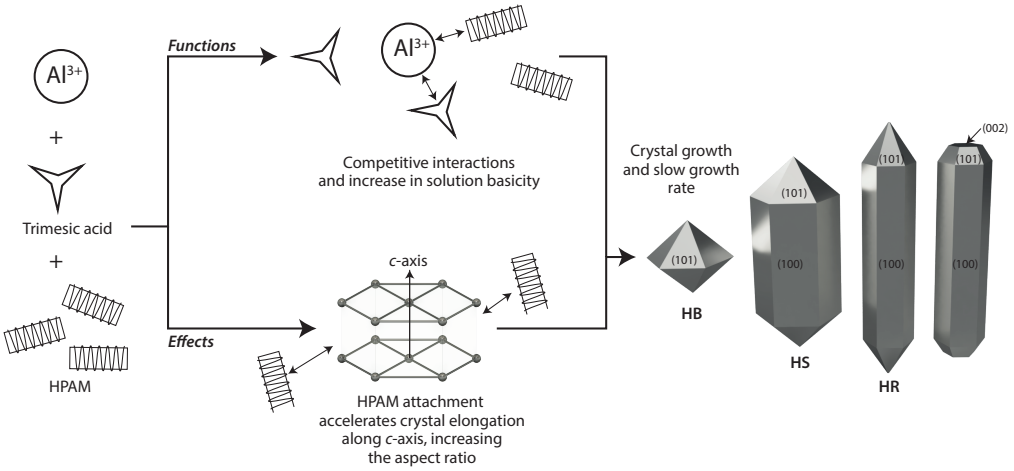

Scheme 1. Schematic mechanism for size and morphology-tunable synthesis of MIL-96 with HPAM in the system.

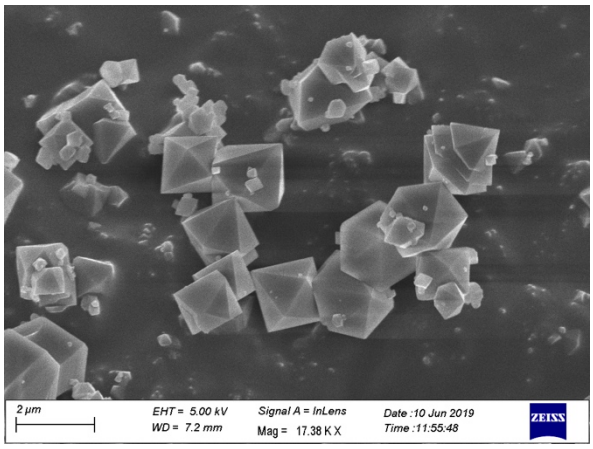

Figure 1. MIL-96 (R_{HPAM} = 0) showing small hexagonal bipyramidal shaped (HB) crystals.

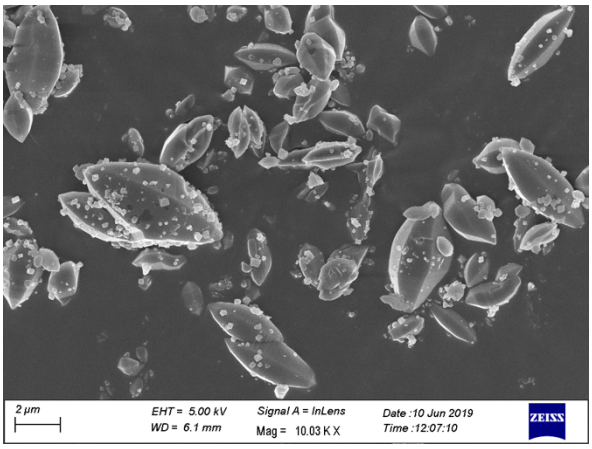

Figure 2. MIL-96 with 2 mL HPAM (R_{HPAM} = 0.2) shows the beginning of hexagonal spindles (HS) crystal growth.

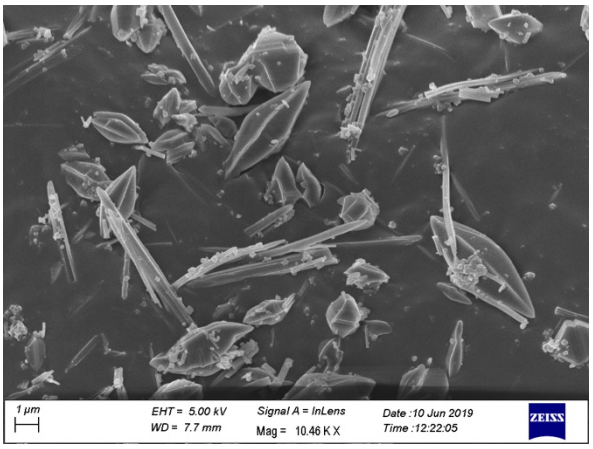

Figure 3. MIL-96 with 6 mL HPAM (R_{HPAM} = 0.6) is a polydisperse mix of HS and elongated hexagonal rods (HR).

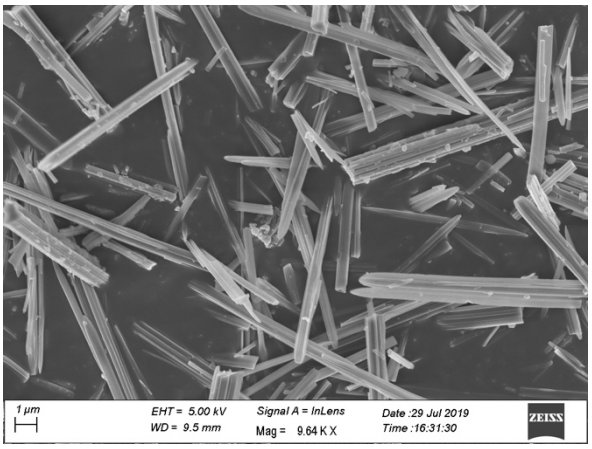

Figure 4. MIL-96 with 20 mL HPAM (R_{HPAM} = 2) showing complete crystal transformation to HR.

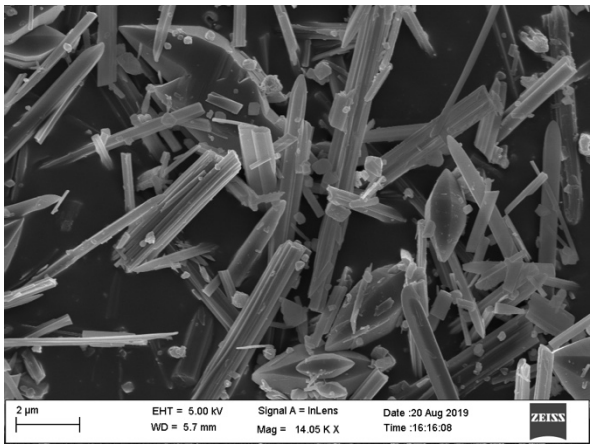

Figure 5. MIL-96 with 20 mL PAM (R_{PAM} = 2) is a mix of a higher proportion of HR than SS crystals.

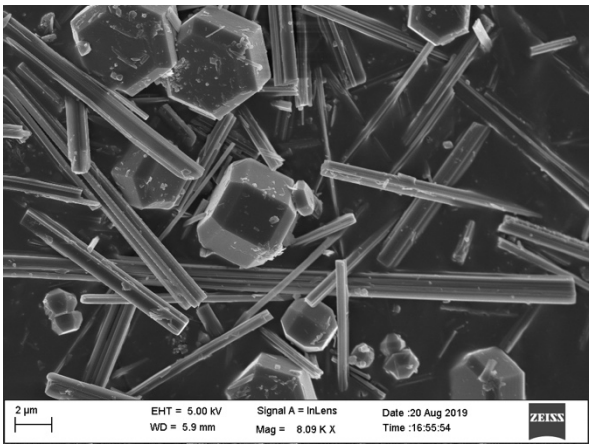

Figure 6. MIL-96 with 20 mL Na-PAA (R_{PAA} = 2) results in the appearance of mixed size hexagonal lumps (HL) alongside HR.

PXRD. As shown in Figure 7, the PXRD patterns of every sample are slightly different compared to the simulated MIL-96 spectra. The peaks have also been shifted slightly to higher

angle. The drift may be attributed to the presence of free TMA inside the pores of the samples.[59] The aforementioned series of crystal shape changes can be defined using the Bravais, Frisdel, Donnay and Harker (BFDH) theory which describes the three main planes that make up the morphology of MIL-96; they are (002), (100) and (101) at 2θ = 5.7°, 7.1° and 7.7° respectively.[39] Except for the subtly present (002), other key characteristic peaks including (102), match well with the simulated spectra, indicating the core crystalline structure is retained. Although by visual inspection, MIL-110 was mainly present at higher HPAM loading as evident by the HR formation, due to instrument limitation (minimum $2\theta \geq 5°$), the characteristic XRD peaks of MIL-100 (2θ = 4°) and MIL-110 ((001) facet; 2θ = 5°)[60] cannot be clearly detected and thus, have to be omitted from subsequent discussion.

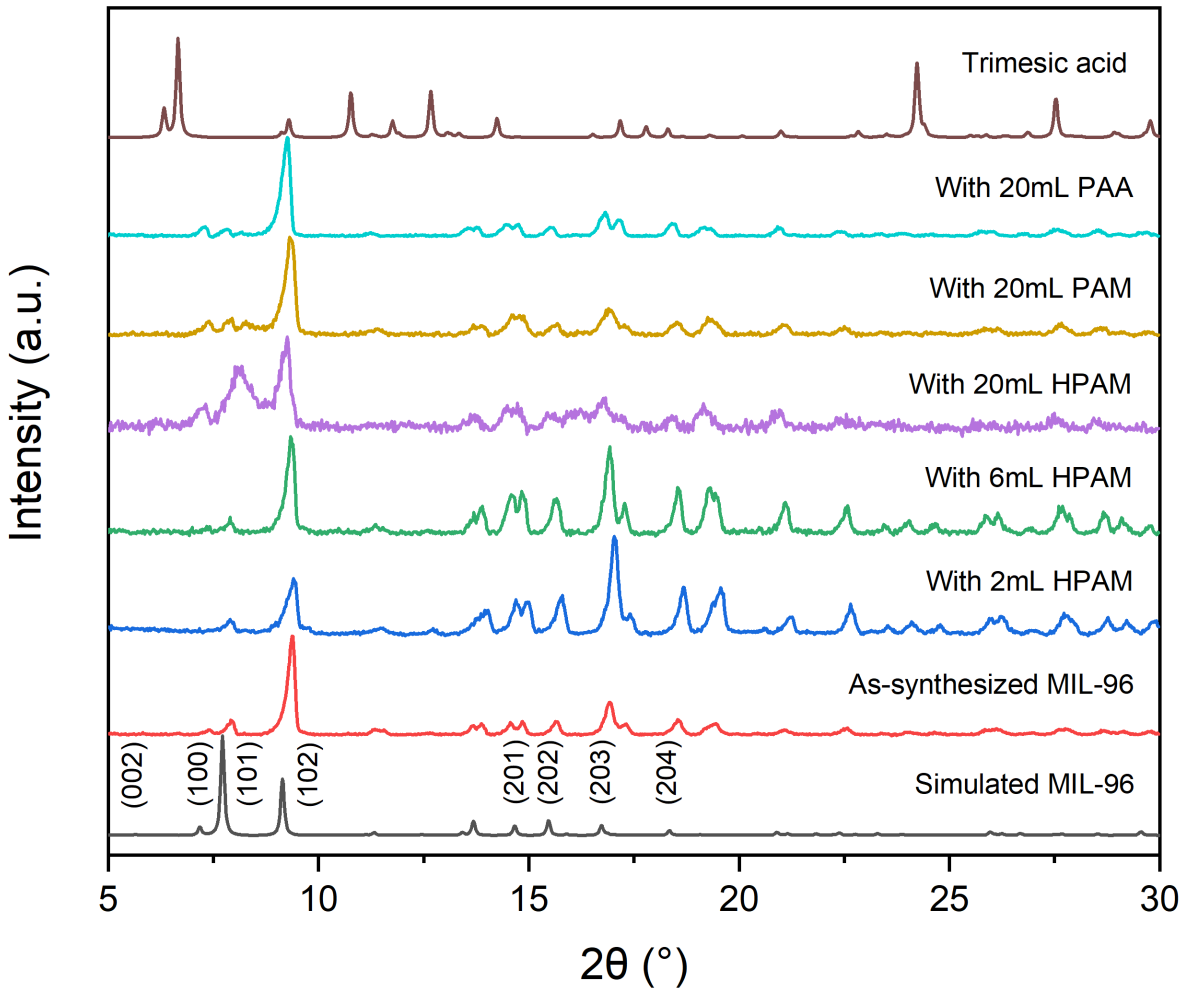

Figure 7. PXRD patterns of the simulated MIL-96 compared to the as-synthesized MIL-96 samples modified with different types and proportions of polymers.

With higher concentration of HPAM, the emerging (100) facet indicates it could enhance the growth rate of the (100), resulting in narrowed edge and the lengthening of the crystals. Furthermore, higher proportion of HPAM accentuates the growth of the (101) crystal plane as shown by the gradual peak increase in which alongside with (100), completes the formation of HR crystal morphology. This is consistent with the reported SEM images. The -NH_2 groups in HPAM function like OH^- ions, increasing solution basicity and speeding up the growth rate along the (101) facet, consequently forming the HR habit.[60]

After the addition of Na-PAA, the (002) facet that is responsible for the formation of HL is only weakly observed in the PXRD, as with the simulated MIL-96, which is probably affected by instrument background noise during scanning, impure phase with ill-defined morphology and powder size inconsistency. Although the BFDH theory also states that the growth rate of the (002) facet to be relatively unaffected, the number of products containing the (002) plane may be subservient compared to the bulk phase which is dominated with (100) and (101)-directed crystals. In short, the preferential crystal growth along the (100) and (101) planes, as a function of higher polymer concentrations, transformed the crystal anisotropy by promoting crystal elongation from its original HB shape. For a hexagonal lattice system, the impact of polymer presence in the reacting environment accelerated the growth along the *c* axis.[54] Moreover, with a higher quantity of added polymers, the subtle width broadening of the strongest peak corresponding to the (102) crystal face implies a slight decrease in particle size. In addition, the relative Bragg peaks of (200) and (201) also become broader and less intense compared to the original MIL-96, supporting the minor reduction in particle size and crystallinity.

FTIR. FTIR spectroscopy was used to understand PFOA adsorption mechanism onto MIL-96-RHPAM2 and the linker interaction with added polymer (Figure S5). Detailed analysis of the IR peaks is displayed in Table 1. The collected spectra of spent MIL-96-RHPAM2 in Figure 8 confirms that PFOA was adsorbed through electrostatic interaction with the MOF. A previous study also inferred the increased intensities of ν_s to ν_{as}(COO) after PFOA adsorption in relation to an inner-sphere complexation with the metal centers. In this case, the carboxylate head groups of PFOA may have formed covalent bond to the surface of MIL-96-RHPAM2.[61]

Table 1. Band assignments for FTIR spectra obtained for MIL-96 samples synthesized with different type and quantity of polymers including HPAM, PAM and Na-PAA.

Wavenumber (cm^{-1})	Mode assignment	Description	Reference
1620	C-H and primary amine N-H in-plane bending.	HPAM and PAM polymers are grafted to the MOF by H-bonding given the newly formed bands.	[62,63]
1570	Asymmetric v_{as} (COO) and v_{as} (C-H) stretching.	Newly formed bands when polymers are added indicate strengthened H-bonding between the carboxylate radical and C-H groups. The peaks might also be super positioned from the N-H in plane bending.	[64,65]
1455 – 1500	Symmetric v_s (COO) stretching.	The characteristic v_s(COO) vibration weakened upon addition of polymers suggesting change in vibration mode to asymmetric.	
1300	Stretching of Al-OH.	Coordinated TMA to the aluminum atoms.	[66]
1146	$v_s(CF_2)$.	Interaction between all characteristic peaks ascribed to PFOA molecules and the MOF.	[61]
1204	$v_{as}(CF_2) + v_{as}(CF_3)$.		
1238	v_{as} (CF_2).		
1319, 1364	$v_{ax}(CF_2)$.		

v_{as}, asymmetric stretch; v_s, symmetric stretch; v_{ax}, axial stretch.

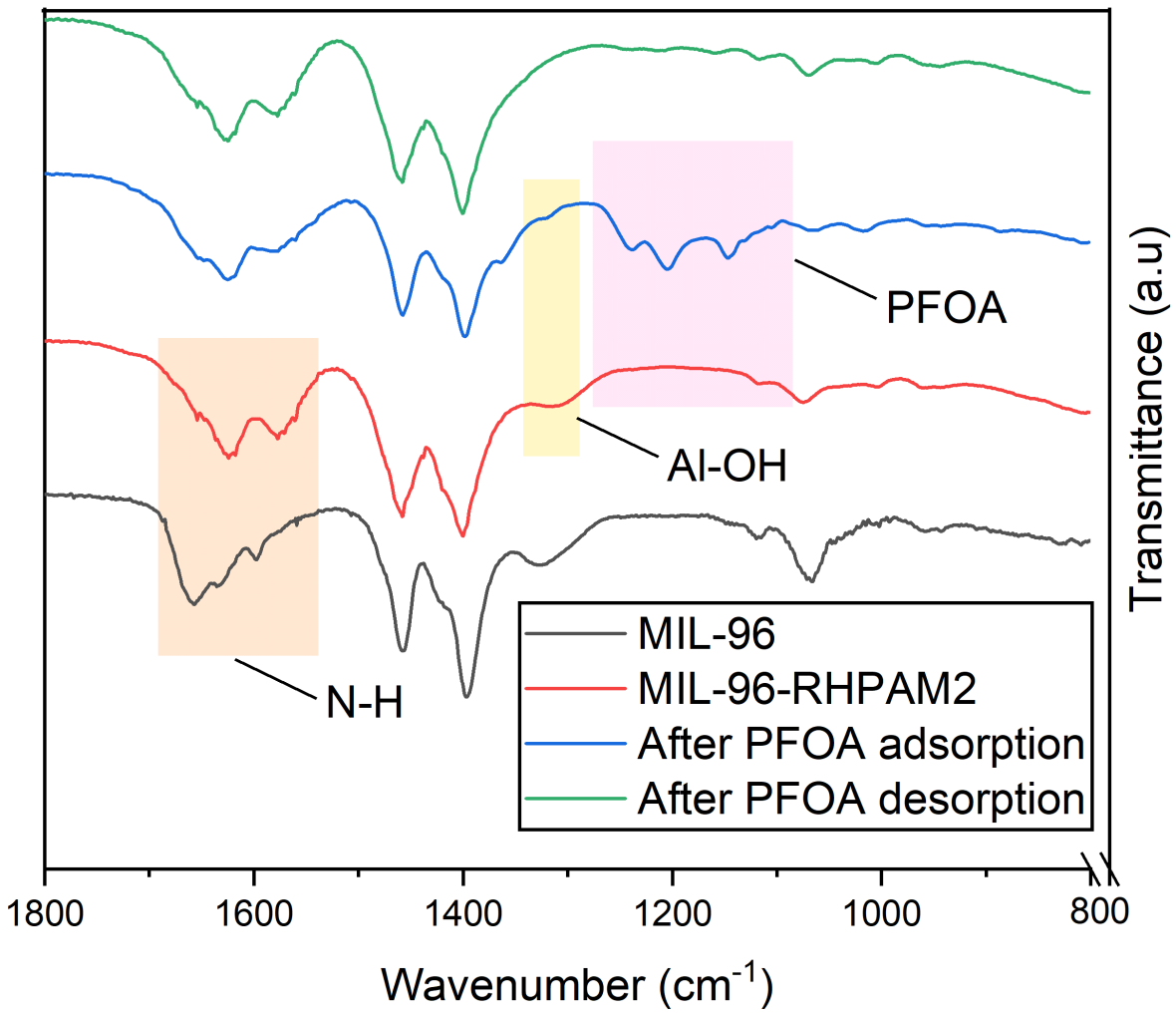

Figure 8. FTIR spectra for the parent MIL-96 and MIL-96-RHPAM2 before and after PFOA adsorption.

BET. The use of PAM, Na-PAA and HPAM for this particle size modification led to a significant reduction in the apparent surface area (SA_{BET}), see Figure 9. The pore size distribution plot in Figure S6 clearly proves complete pore blocking when HPAM was used, asserting its location inside the pores. Interestingly, compared to the apparent surface area of AC (SA_{BET} = 1179 m^2/g), MIL-96-

RHPAM2 (SA_{BET} = 75 m^2/g) has comparatively good PFOA adsorption capacity even though it possesses a lower surface area.

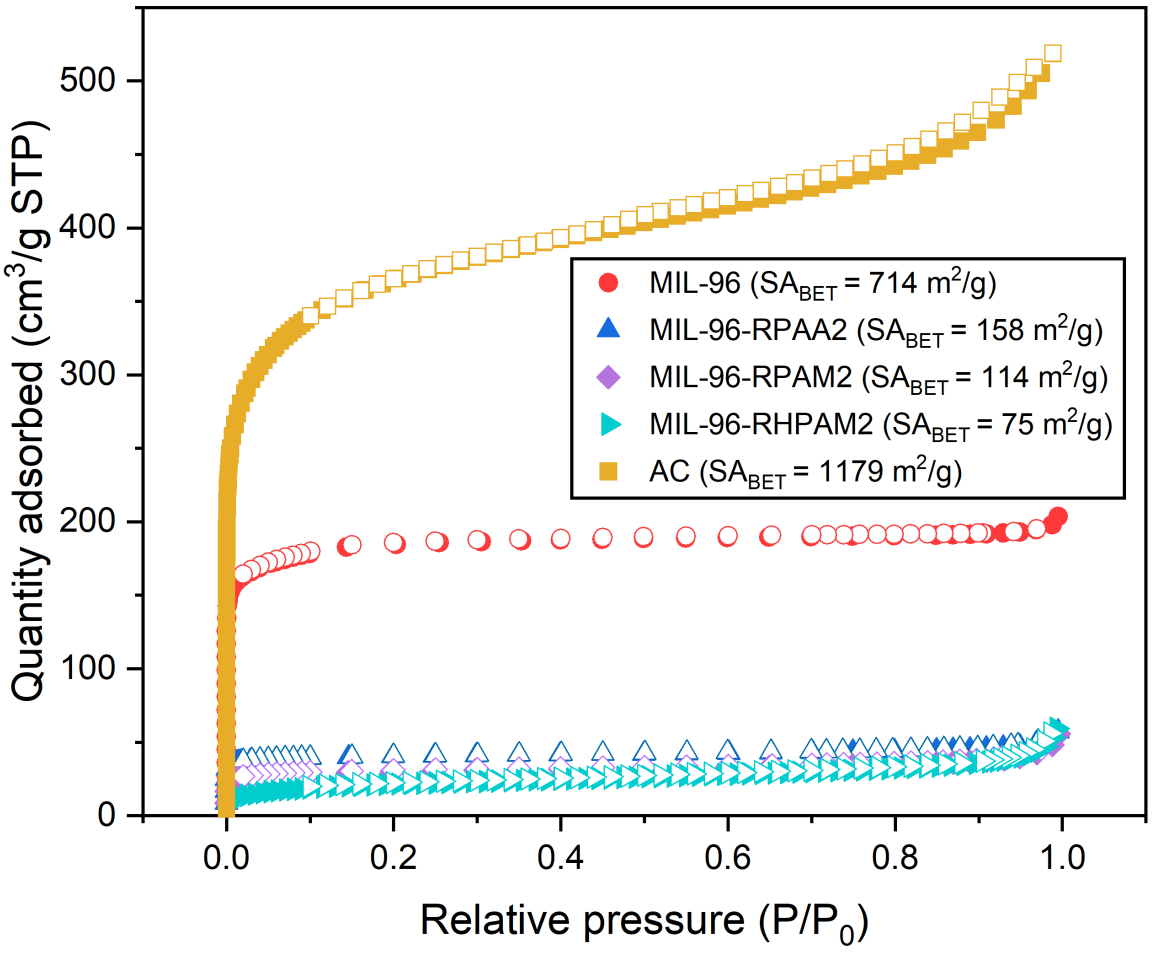

Figure 9. N_2 adsorption and desorption isotherms performed at 77 K on AC and all modified MIL-96 materials. Filled symbols ■ denote adsorption whereas unfilled symbols □ denote desorption.

Adsorption Kinetics. Apart from knowing the equilibrium adsorption capacity of sorbents (Figure S9), it is equally important to understand the adsorption kinetics involved in the PFOA removal by MIL-96-RHPAM2. Based on previous studies, the experimental data obtained herein is fitted using a pseudo second order (PSO) kinetic model. Figure 11 highlights the severe diffusion

limitation exhibited by MIL-96-RHPAM2 as the material's adsorptive capacity only reached its plateau after 186 hours of contact time. Concurrently, the PFOA adsorption data can also be described by the Elovich kinetic model. Non-linear plots using both models showed high regression coefficients with PSO (R^2 = 0.983) and Elovich (R^2 = 0.996), suggesting chemisorption is the rate limiting step as supported by the FTIR analysis. Since the Elovich equation gave superior approximation to the experimental data, it may be concluded that the adsorption proceeded in a highly heterogenous system.[67] Earlier discussions have highlighted the abundance of chemical functional groups comprising of -NH_2, -OH, -COOH, -NH_3^+ and the Al^{3+} metal centers on MIL-96-RHPAM2 which may readily bind to PFOA.

To gain a detailed insight in the PFOA adsorption kinetics for MIL-96-RHPAM2, vapor phase adsorption experiments were conducted with a hydrocarbon analogue to PFOA; n-octane (C_8H_{18}) (Figure S11 – S12). The fundamental differences in liquid-phase adsorption and vapor adsorption are acknowledged but, in both cases, the kinetic rate is nonetheless similar (denoted by the proximity of $k_2 = 2 \times 10^{-4}$ g/mg.min). Vapor phase adsorption time of 1000 minutes is still insufficient to realize an equilibrium adsorption state. The BET result shows that although increasing the HPAM content increases the particle size (Figure 10 and Table 2), it has compromised the material's porosity. In turn, there is an increase in the diffusion path length inside the adsorbent that hindered effective diffusion and prolonging the time required to reach equilibrium.[68] It may appear that the approach outlined here has created another problem but, there is a future opportunity to retain the beneficial effect provided by HPAM by tuning MIL-96 adsorption capacity with temperature, taking into account the high thermal stability of HPAM[69] and the flexibility of changing, increasing, its pore size.[70]

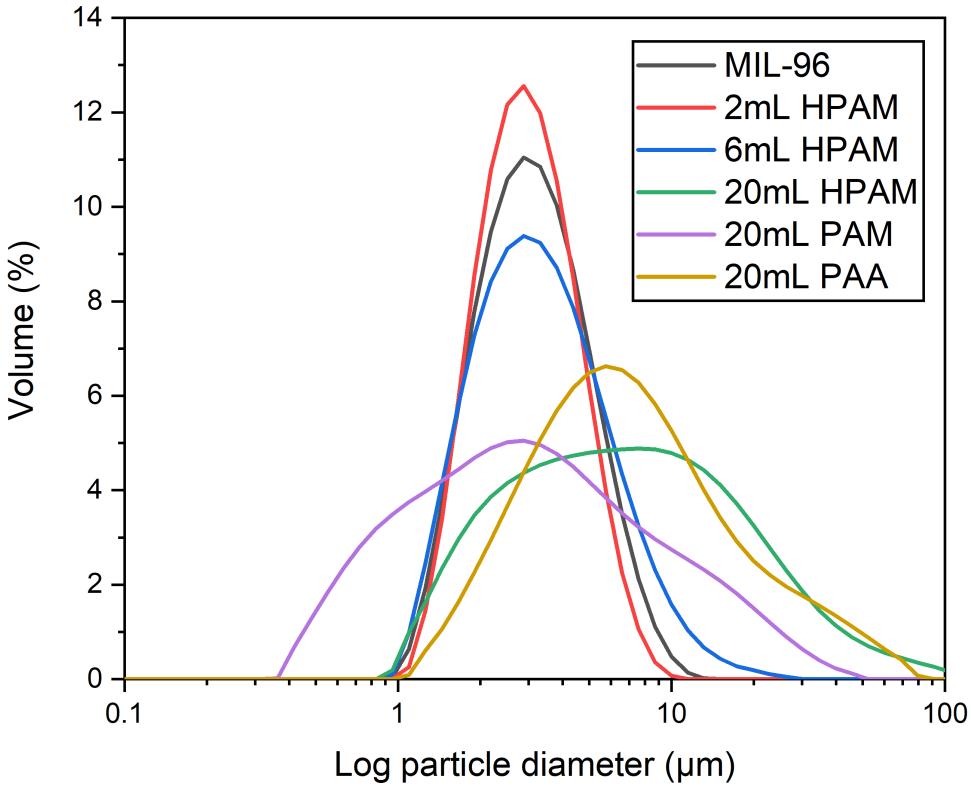

Figure 10. Hydrated particle size distribution (diameter in μm) of polymer-modified MIL-96 in pure water by laser light diffraction. The particle size ranges shown reflect the true size as particles were pre-sonicated prior to the laser light diffraction measurement.

Table 2. Measured hydrodynamic particle diameter (n = 5) for polymer modified MIL-96 samples. Addition of 20 mL HPAM effectively formed the largest MIL-96 particles, showing over 200% diameter increase from 3.2 μm to 10.4 μm.

Sample name	Volume weighted mean particle diameter (μm)
MIL-96 (R_{HPAM} = 0)	3.2
MIL-96 modified with 2 mL HPAM (R_{HPAM} = 0.2)	3.0
MIL-96 modified with 6 mL HPAM (R_{HPAM} = 0.6)	3.7
MIL-96 modified with 20 mL HPAM (R_{HPAM} = 2)	10.4
MIL-96 modified with 20 mL PAM (R_{PAM} = 2)	5.0
MIL-96 modified with 20 mL Na-PAA (R_{PAA} = 2)	9.9

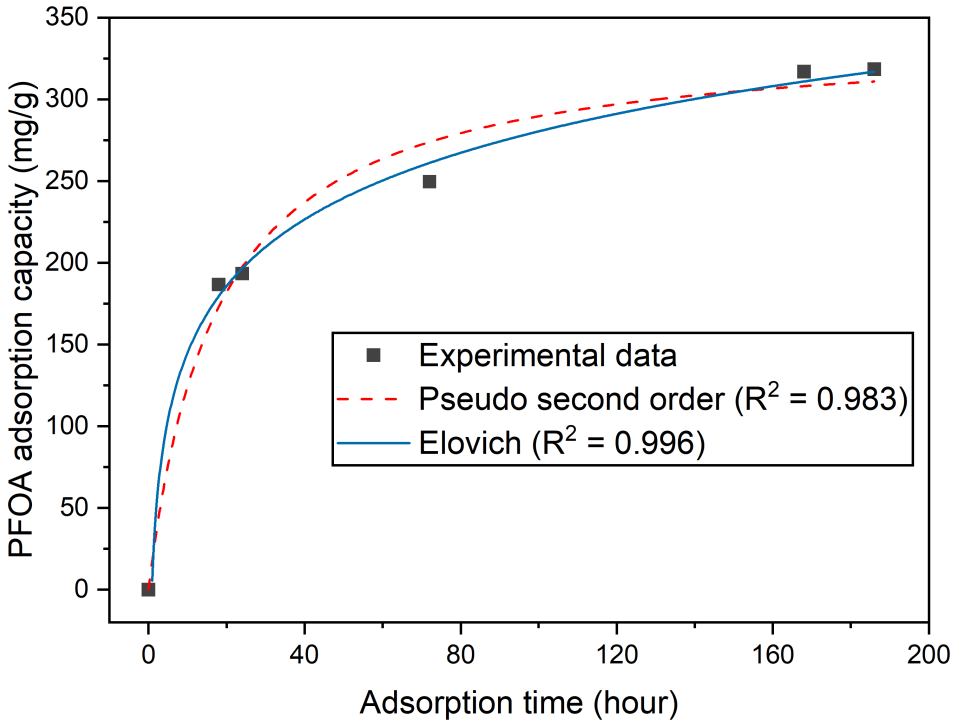

Figure 11. Experimental and kinetic modelling results for the adsorptive PFOA removal by MIL-96-RHPAM2; [PFOA] = 1000 mg/L, [MOF] = 1 mg/mL.

In comparison to the reported kinetic data for PFOA removal by several other adsorbents, MIL-96-RHPAM2 can adsorb PFOA at loading levels on a par with other adsorbents, but the extremely slow uptake would be a significant drawback for its practical use. Relative to other adsorption studies displayed in Table 3, the PFOA concentration used in this work is the highest.

Table 3. Comparison of the pseudo-second order kinetic parameters for PFOA adsorption by select MOFs and AC.

Sorbent used	Tested PFOA concentration (mg/L)	Pseudo-second order model parameter			Equilibrium time (hr)	Reference
		q_e (mg/g)	k_2 (g/mg.min)	R^2		
Bamboo-derived AC	120	393	2.7×10^{-5}	0.91	33.5	[20]
Fe_3O_4-modified AC	300	364	7.1×10^{-5}	0.998	29	[21]
Perfluorinated UiO-66-(F4)	500	381	2.6×10^{-3}	0.993	1	[28]
UiO-66		327	2.7×10^{-3}	0.996		
MIL-101 (Cr)	100	481	1.4×10^{-4}	0.967	1	[29]
Quaternized amine MIL-101 (Cr)-QDMEN		791	2.1×10^{-4}	0.985		
MIL-53 (Al)	1	100	7.3×10^{-2}	0.999	4	[30]
ZIF-7	-	22	7.1×10^{-5}	0.994	1	[31]
ZIF-8		177	2.0×10^{-5}	0.978		
ZIF-L		244	9.6×10^{-6}	0.985		
UiO-67	500	350	6.1×10^{-4}	0.999	1	[32]

MIL-96-RHPAM2	1000	340*	1.7×10^{-4}	0.983	186	This work

*Shows the increase in adsorption capacity after kinetic experiment was extended to 186 hours suggesting MIL-96-RHPAM2 has a very slow kinetic rate.

PFOA Adsorption and Desorption. Knowing that PFCs are hazardous chemicals, safe regeneration and economical reuse of the spent adsorbents is critically important. Although thermal regeneration is preferably used by carbon manufacturers, adsorbed PFCs are not easily removed from the carbon surfaces by decomposition as C-F is the strongest single bond in organic chemistry after B-F, Si-F and H-F. While the next best alternative is to use higher regeneration temperatures to break the C-F bond, this often results in high carbon losses.[18]

To develop an efficient PFOA regeneration method from spent MOF, the nature of adsorption processes must first be understood. An earlier report on PFOA adsorption by MOF had confirmed the electrostatic interaction between the cationic MOF species (Al^{3+}) with the anionic carboxylate groups (COO^-) of PFOA as the main binding mechanism, supplemented by H-bonding and hydrophobic interaction to a lesser extent.[30] So, with electrostatic interaction being the most prevalent, it was decided to trial saline eluents to evaluate their destabilization effect on the electrostatic PFOA adsorption complex.

The positively charged Al^{3+} center of MIL-96 is surmised to have a strong interaction with the anionic carboxylate groups (COO^-) of PFOA. Contrary to expectations, increasing the eluent ionic strength has minimal effect on PFOA desorption by MIL-96-RHPAM2[22,23] except for a slight drop at the highest tested salt concentration (500 mM NaCl). Such salt concentration may be sufficiently

high enough to reduce the electrostatic forces between the Al^{3+} center and the negatively charged PFOA molecules resulting from the competitive PFOA adsorption with the background ions (Na^+ and Cl^-).[61] However, due to the well-established acid-base and electrostatic bonds between the Al^{3+}, carboxylate (COO^-), hydroxyl (OH), NH_2 and NH_3^+ functional groups on the MOF, the driving force to establish new bonds with the incoming Na^+ and Cl^- ions is not as favorable, hence, not accommodating the desorption of adsorbed PFOA molecules into the eluent phase.

Apart from the Al^{3+} center being a major MOF binding site, it is probable that the NH_2, which will also exist in a protonated form as a NH_3^+, contained in HPAM also attaches to the anionic carboxylate of PFOA via strong electrostatic adsorption forces.[29,71] In addition, the van der Waals interaction between the carbon chain of PFOA (8 carbons on the PFOA) and the main skeleton $(CH_2\text{-}CH)_n$ of HPAM may also contribute to the adsorption process. Altogether, these explanations for the incomplete desorption of PFOA from aminated adsorbents such as MIL-96-RHPAM2 are in line with the obtained result from batch desorption studies. Figure 12 illustrates the nuanced NaCl influence in the eluent to the PFOA desorption performance of MIL-96-RHPAM2. Across the tested salinity window, the highest PFOA fraction desorbed only reached 77% but not full recovery, providing future research opportunities to clarify the best solvent/ salt systems capable of complete PFOA desorption. Descriptions on the possible PFOA adsorption mechanisms onto MIL-96-RHPAM2 can be found in Figure S14 (Scheme S1) and Figure S15 (Scheme S2) for the pristine form.

Although PFOA desorption efficiency from AC is inferior to MIL-96-RHPAM2 at lower ionic strengths, AC's desorption efficiency is improved at the highest ionic strength tested here. Similar

to MOF, PFOA adsorption onto AC shares similar adsorption mechanisms,[22,72] confirming the importance of surface chemistry on AC. There is a clear correlation with a marked increase in PFCs sorption with more availability of basic groups in the adsorbents. Thus, to enhance the adsorption process, an abundance of hydroxyl and carboxyl oxygen-containing functional groups on the AC surface will then interact with the PFOA anions via acid-base/electrostatic interactions.[73] Along the same lines, the oxygen-containing basic and acidic surface groups on AC may form H-bond interactions with the amphoteric COOH functional groups within PFOA. An increase in the eluent ionic strength can potentially weaken these PFOA to AC H-bonding interactions by the Na^+ and the Cl^- ions shielding the electrostatic interactions whilst also directly competing for the H-bonding sites. While these results show that NaCl was not an effective PFOA desorption facilitating agent, only catalytic degradation has so far offered superior performance.[19,74]

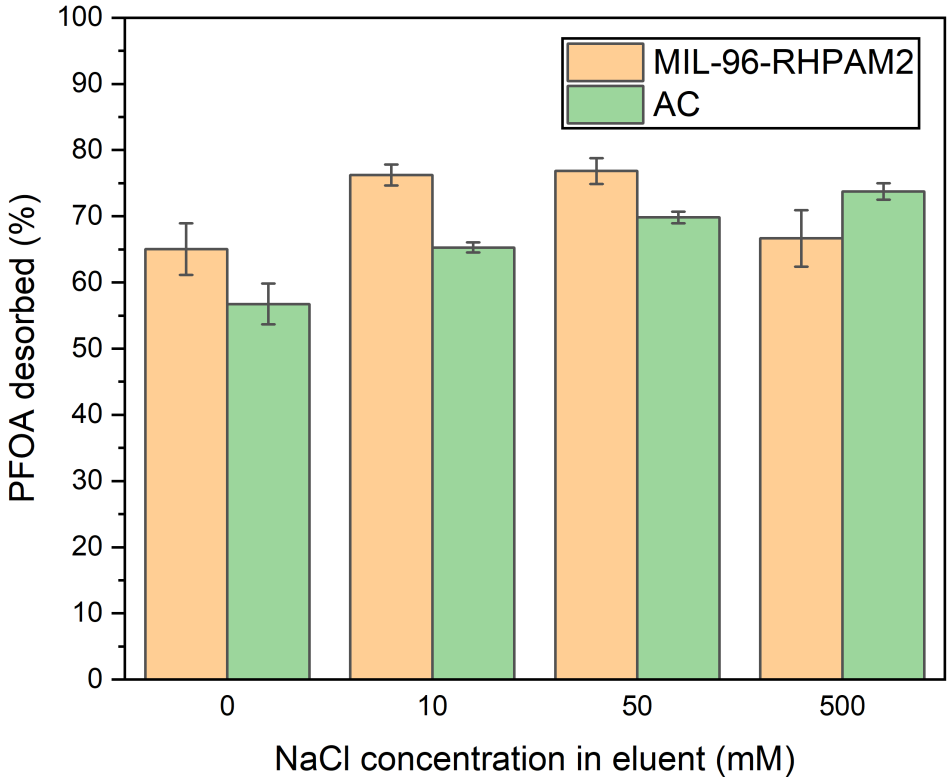

Figure 12. Percentage of PFOA desorbed from MIL-96-RHPAM2 and AC using eluents with various NaCl concentrations (temperature 25 °C, adsorbent dose = 2 mg/L, initial PFOA concentration = 1000 mg/L).

4. Conclusions

The addition of an anionic polymer (HPAM) to a cationic aluminum-based MOF (MIL-96) during the hydrothermal synthesis stage allowed the formation of larger MOF crystals with well-defined crystal habits. Taking advantage of HPAM being a low cost and an environmentally friendly

additive, a HPAM-modified MIL-96 (MIL-96-RHPAM2) showed promising particle size growth (from 3.2 μm to 10.4 μm) as well as the ability to control the crystal morphology using this simple modification procedure. Incorporating HPAM into the MIL-96 structure resulted in the introduction of amine ($-NH_2$) functionality, which can form a primary ammonium species ($-NH_3^+$) that in turn led to improved PFOA adsorption capacity relative to original pristine form, while also promoting higher PFOA affinity compared to AC. Higher concentrations of NaCl in the eluent solvents did not yield enhanced PFOA desorption from both spent adsorbents, MIL-96-RHPAM2 (maximum PFOA desorbed was 77%) and AC (74%), primarily due to the strong PFOA adsorption to both adsorbents.

Associated Content

Supporting Information. SEM images of HPAM-modified MIL-101 (Cr), IR spectra analysis of HPAM-treated linker, data pertaining to sample's pore size distribution, TGA-MS, batch adsorption, n-octane vapor sorption study, particle size measurements, elemental analysis, and illustration of PFOA adsorption mechanisms by MIL-96-RHPAM2 are included. The raw data presented in all Figures, and high-resolution versions of the SEM images, are available from the open repository https://doi.org/10.5281/zenodo.3839252

Author Information

Corresponding Author. Bradley Ladewig - Institute for Micro Process Engineering (IMVT), Karlsruhe Institute of Technology, Hermann-von-Helmholtz-Platz 1, 76344 Eggenstein-Leopoldshafen, Germany; email: bradley.ladewig@kit.edu.

Author Contributions. All authors have consented to the final version of the manuscript.

Notes. The authors declare no competing financial interest.

Acknowledgment

Luqman Hakim Mohd Azmi gratefully acknowledges the financial support by the sovereign wealth fund of Malaysian Government, Yayasan Khazanah for his PhD studies.

References

(1) Tiedeken, E. J.; Tahar, A.; McHugh, B.; Rowan, N. J. Monitoring, Sources, Receptors, and Control Measures for Three European Union Watch List Substances of Emerging Concern in Receiving Waters – A 20 Year Systematic Review. *Sci. Total Environ.* **2017**, *574*, 1140–1163. https://doi.org/10.1016/j.scitotenv.2016.09.084.

(2) Rivera-Utrilla, J.; Sánchez-Polo, M.; Ferro-García, M. Á.; Prados-Joya, G.; Ocampo-Pérez, R. Pharmaceuticals as Emerging Contaminants and Their Removal from Water. A Review. *Chemosphere* **2013**, *93* (7), 1268–1287. https://doi.org/10.1016/j.chemosphere.2013.07.059.

(3) Cordner, A.; Vanessa, Y.; Schaider, L. A.; Rudel, R. A.; Richter, L.; Brown, P. Guideline Levels for PFOA and PFOS in Drinking Water: The Role of Scientific Uncertainty, Risk Assessment Decisions, and Social Factors. *J. Expo. Sci. Environ. Epidemiol.* **2019**, *29* (2), 157.

(4) Valsecchi, S.; Conti, D.; Crebelli, R.; Polesello, S.; Rusconi, M.; Mazzoni, M.; Preziosi, E.; Carere, M.; Lucentini, L.; Ferretti, E. Deriving Environmental Quality Standards for Perfluorooctanoic Acid (PFOA) and Related Short Chain Perfluorinated Alkyl Acids. *J. Hazard. Mater.* **2017**, *323*, 84–98.

(5) Li, L.; Zheng, H.; Wang, T.; Cai, M.; Wang, P. Perfluoroalkyl Acids in Surface Seawater from the North Pacific to the Arctic Ocean: Contamination, Distribution and Transportation. *Environ. Pollut.* **2018**, *238*, 168–176.

(6) Scher, D. P.; Kelly, J. E.; Huset, C. A.; Barry, K. M.; Hoffbeck, R. W.; Yingling, V. L.;

Messing, R. B. Occurrence of Perfluoroalkyl Substances (PFAS) in Garden Produce at Homes with a History of PFAS-Contaminated Drinking Water. *Chemosphere* **2018**, *196*, 548–555.

(7) Andersson, E. M.; Scott, K.; Xu, Y.; Li, Y.; Olsson, D. S.; Fletcher, T.; Jakobsson, K. High Exposure to Perfluorinated Compounds in Drinking Water and Thyroid Disease. A Cohort Study from Ronneby, Sweden. *Environ. Res.* **2019**, *176*, 108540.

(8) Lorenzo, M.; Campo, J.; Suárez-Varela, M. M.; Picó, Y. Occurrence, Distribution and Behavior of Emerging Persistent Organic Pollutants (POPs) in a Mediterranean Wetland Protected Area. *Sci. Total Environ.* **2019**, *646*, 1009–1020.

(9) Feng, X.; Ye, M.; Li, Y.; Zhou, J.; Sun, B.; Zhu, Y.; Zhu, L. Potential Sources and Sediment-Pore Water Partitioning Behaviors of Emerging per/Polyfluoroalkyl Substances in the South Yellow Sea. *J. Hazard. Mater.* **2020**, *389*, 122124.

(10) Richardson, S. D. Environmental Mass Spectrometry: Emerging Contaminants and Current Issues. *Anal. Chem.* **2008**, *80* (12), 4373–4402. https://doi.org/10.1021/ac202903d.

(11) McNamara, J. D.; Franco, R.; Mimna, R.; Zappa, L. Comparison of Activated Carbons for Removal of Perfluorinated Compounds from Drinking Water. *Journal-American Water Work. Assoc.* **2018**, *110* (1), E2–E14.

(12) Hu, X. C.; Andrews, D. Q.; Lindstrom, A. B.; Bruton, T. A.; Schaider, L. A.; Grandjean, P.; Lohmann, R.; Carignan, C. C.; Blum, A.; Balan, S. A. Detection of Poly-and Perfluoroalkyl Substances (PFASs) in US Drinking Water Linked to Industrial Sites, Military Fire Training Areas, and Wastewater Treatment Plants. *Environ. Sci. Technol. Lett.* **2016**, *3* (10), 344–

350.

(13) Sunderland, E. M.; Hu, X. C.; Dassuncao, C.; Tokranov, A. K.; Wagner, C. C.; Allen, J. G. A Review of the Pathways of Human Exposure to Poly-and Perfluoroalkyl Substances (PFASs) and Present Understanding of Health Effects. *J. Expo. Sci. Environ. Epidemiol.* **2019**, *29* (2), 131–147.

(14) Piekarski, D. J.; Diaz, K. R.; McNerney, M. W. Perfluoroalkyl Chemicals in Neurological Health and Disease: Human Concerns and Animal Models. *Neurotoxicology* **2020**.

(15) Rashtian, J.; Chavkin, D. E.; Merhi, Z. Water and Soil Pollution as Determinant of Water and Food Quality/Contamination and Its Impact on Female Fertility. *Reprod. Biol. Endocrinol.* **2019**, *17* (1), 5.

(16) Huang, M.; Jiao, J.; Zhuang, P.; Chen, X.; Wang, J.; Zhang, Y. Serum Polyfluoroalkyl Chemicals Are Associated with Risk of Cardiovascular Diseases in National US Population. *Environ. Int.* **2018**, *119*, 37–46.

(17) Mancini, F. R.; Cano-Sancho, G.; Gambaretti, J.; Marchand, P.; Boutron-Ruault, M.; Severi, G.; Arveux, P.; Antignac, J.; Kvaskoff, M. Perfluorinated Alkylated Substances Serum Concentration and Breast Cancer Risk: Evidence from a Nested Case-control Study in the French E3N Cohort. *Int. J. Cancer* **2020**, *146* (4), 917–928.

(18) Ateia, M.; Maroli, A.; Tharayil, N.; Karanfil, T. The Overlooked Short-and Ultrashort-Chain Poly-and Perfluorinated Substances: A Review. *Chemosphere* **2019**, *220*, 866–882.

(19) Du, Z.; Deng, S.; Bei, Y.; Huang, Q.; Wang, B.; Huang, J.; Yu, G. Adsorption Behavior and

Mechanism of Perfluorinated Compounds on Various Adsorbents—a Review. *J. Hazard. Mater.* **2014**, *274*, 443–454.

(20) Du, Z.; Deng, S.; Chen, Y.; Wang, B.; Huang, J.; Wang, Y.; Yu, G. Removal of Perfluorinated Carboxylates from Washing Wastewater of Perfluorooctanesulfonyl Fluoride Using Activated Carbons and Resins. *J. Hazard. Mater.* **2015**, *286*, 136–143.

(21) Xu, J.; Liu, Z.; Zhao, D.; Gao, N.; Fu, X. Enhanced Adsorption of Perfluorooctanoic Acid (PFOA) from Water by Granular Activated Carbon Supported Magnetite Nanoparticles. *Sci. Total Environ.* **2020**, 137757.

(22) Wang, F.; Shih, K. Adsorption of Perfluorooctanesulfonate (PFOS) and Perfluorooctanoate (PFOA) on Alumina: Influence of Solution PH and Cations. *Water Res.* **2011**, *45* (9), 2925–2930.

(23) Shih, K.; Wang, F. Adsorption Behavior of Perfluorochemicals (PFCs) on Boehmite: Influence of Solution Chemistry. *Procedia Environ. Sci.* **2013**, *18*, 106–113.

(24) Badruddoza, A. Z. M.; Bhattarai, B.; Suri, R. P. S. Environmentally Friendly β-Cyclodextrin–Ionic Liquid Polyurethane-Modified Magnetic Sorbent for the Removal of PFOA, PFOS, and Cr (VI) from Water. *ACS Sustain. Chem. Eng.* **2017**, *5* (10), 9223–9232.

(25) Xiao, L.; Ling, Y.; Alsbaiee, A.; Li, C.; Helbling, D. E.; Dichtel, W. R. β-Cyclodextrin Polymer Network Sequesters Perfluorooctanoic Acid at Environmentally Relevant Concentrations. *J. Am. Chem. Soc.* **2017**, *139* (23), 7689–7692. https://doi.org/10.1021/jacs.7b02381.

(26) Yang, Y.; Ding, Q.; Yang, M.; Wang, Y.; Liu, N.; Zhang, X. Magnetic Ion Exchange Resin for Effective Removal of Perfluorooctanoate from Water: Study of a Response Surface Methodology and Adsorption Performances. *Environ. Sci. Pollut. Res.* **2018**, *25* (29), 29267–29278.

(27) Ateia, M.; Attia, M. F.; Maroli, A.; Tharayil, N.; Alexis, F.; Whitehead, D. C.; Karanfil, T. Rapid Removal of Poly-and Perfluorinated Alkyl Substances by Poly (Ethylenimine)-Functionalized Cellulose Microcrystals at Environmentally Relevant Conditions. *Environ. Sci. Technol. Lett.* **2018**, *5* (12), 764–769.

(28) Sini, K.; Bourgeois, D.; Idouhar, M.; Carboni, M.; Meyer, D. Metal-Organic Framework Sorbents for the Removal of Perfluorinated Compounds in an Aqueous Environment. *New J. Chem.* **2018**, *42* (22), 17889–17894. https://doi.org/10.1039/c8nj03312a.

(29) Liu, K.; Zhang, S.; Hu, X.; Zhang, K.; Roy, A.; Yu, G. Understanding the Adsorption of PFOA on MIL-101 (Cr)-Based Anionic-Exchange Metal–Organic Frameworks: Comparing DFT Calculations with Aqueous Sorption Experiments. *Environ. Sci. Technol.* **2015**, *49* (14), 8657–8665.

(30) Jun, B.-M.; Hwang, H. S.; Heo, J.; Han, J.; Jang, M.; Sohn, J.; Park, C. M.; Yoon, Y. Removal of Selected Endocrine-Disrupting Compounds Using Al-Based Metal Organic Framework: Performance and Mechanism of Competitive Adsorption. *J. Ind. Eng. Chem.* **2019**, *79*, 345–352.

(31) Chen, M.-J.; Yang, A.-C.; Wang, N.-H.; Chiu, H.-C.; Li, Y.-L.; Kang, D.-Y.; Lo, S.-L. Influence of Crystal Topology and Interior Surface Functionality of Metal-Organic

Frameworks on PFOA Sorption Performance. *Microporous Mesoporous Mater*. **2016**, *236*, 202–210.

(32) Sini, K.; Bourgeois, D.; Idouhar, M.; Carboni, M.; Meyer, D. Metal-Organic Frameworks Cavity Size Effect on the Extraction of Organic Pollutants. *Mater. Lett*. **2019**, *250*, 92–95.

(33) Vecitis, C. D.; Park, H.; Cheng, J.; Mader, B. T.; Hoffmann, M. R. Treatment Technologies for Aqueous Perfluorooctanesulfonate (PFOS) and Perfluorooctanoate (PFOA). *Front. Environ. Sci. Eng. China* **2009**, *3* (2), 129–151.

(34) Xue, H.; Chen, Q.; Jiang, F.; Yuan, D.; Lv, G.; Liang, L.; Liu, L.; Hong, M. A Regenerative Metal–Organic Framework for Reversible Uptake of Cd (II): From Effective Adsorption to in Situ Detection. *Chem. Sci*. **2016**, *7* (9), 5983–5988.

(35) Gebald, C.; Repond, N.; Ruesch, T.; Wurzbacher, J. A. Low-Pressure Drop Structure of Particle Adsorbent Bed for Adsorption Gas Separation Process. US10427086B2, October 1, 2019.

(36) Mandić, M.; Todić, B.; Živanić, L.; Nikačević, N.; Bukur, D. B. Effects of Catalyst Activity, Particle Size and Shape, and Process Conditions on Catalyst Effectiveness and Methane Selectivity for Fischer–Tropsch Reaction: A Modeling Study. *Ind. Eng. Chem. Res*. **2017**, *56* (10), 2733–2745.

(37) Seoane, B.; Castellanos, S.; Dikhtiarenko, A.; Kapteijn, F.; Gascon, J. Multi-Scale Crystal Engineering of Metal Organic Frameworks. *Coord. Chem. Rev*. **2016**, *307*, 147–187.

(38) Long, P.; Wu, H.; Zhao, Q.; Wang, Y.; Dong, J.; Li, J. Solvent Effect on the Synthesis of

MIL-96 (Cr) and MIL-100 (Cr). *Microporous Mesoporous Mater*. **2011**, *142* (2–3), 489–493.

(39) Liu, D.; Liu, Y.; Dai, F.; Zhao, J.; Yang, K.; Liu, C. Size-and Morphology-Controllable Synthesis of MIL-96 (Al) by Hydrolysis and Coordination Modulation of Dual Aluminium Source and Ligand Systems. *Dalt. Trans*. **2015**, *44* (37), 16421–16429.

(40) Guo, C.; Zhang, Y.; Guo, Y.; Zhang, L.; Zhang, Y.; Wang, J. A General and Efficient Approach for Tuning the Crystal Morphology of Classical MOFs. *Chem. Commun*. **2018**, *54* (3), 252–255.

(41) Han, Y.; Liu, M.; Li, K.; Zuo, Y.; Wei, Y.; Xu, S.; Zhang, G.; Song, C.; Zhang, Z.; Guo, X. Facile Synthesis of Morphology and Size-Controlled Zirconium Metal–Organic Framework UiO-66: The Role of Hydrofluoric Acid in Crystallization. *CrystEngComm* **2015**, *17* (33), 6434–6440.

(42) Wang, F.; Guo, H.; Chai, Y.; Li, Y.; Liu, C. The Controlled Regulation of Morphology and Size of HKUST-1 by "Coordination Modulation Method." *Microporous Mesoporous Mater*. **2013**, *173*, 181–188.

(43) Falcaro, P.; Hill, A. J.; Nairn, K. M.; Jasieniak, J.; Mardel, J. I.; Bastow, T. J.; Mayo, S. C.; Gimona, M.; Gomez, D.; Whitfield, H. J. A New Method to Position and Functionalize Metal-Organic Framework Crystals. *Nat. Commun*. **2011**, *2*, 237.

(44) Yan, X.; Lu, N.; Fan, B.; Bao, J.; Pan, D.; Wang, M.; Li, R. Synthesis of Mesoporous and Tetragonal Zirconia with Inherited Morphology from Metal–Organic Frameworks. *CrystEngComm* **2015**, *17* (33), 6426–6433.

(45) Lee, J.; Kwak, S.-Y. Tubular Superstructures Composed of α-Fe2O3 Nanoparticles from Pyrolysis of Metal–Organic Frameworks in a Confined Space: Effect on Morphology, Particle Size, and Magnetic Properties. *Cryst. Growth Des.* **2017**, *17* (9), 4496–4500.

(46) Vaitsis, C.; Sourkouni, G.; Argirusis, C. Metal Organic Frameworks (MOFs) and Ultrasound: A Review. *Ultrason. Sonochem.* **2019**, *52*, 106–119.

(47) Watanabe, S.; Ohsaki, S.; Hanafusa, T.; Takada, K.; Tanaka, H.; Mae, K.; Miyahara, M. T. Synthesis of Zeolitic Imidazolate Framework-8 Particles of Controlled Sizes, Shapes, and Gate Adsorption Characteristics Using a Central Collision-Type Microreactor. *Chem. Eng. J.* **2017**, *313*, 724–733.

(48) Rellegadla, S.; Prajapat, G.; Agrawal, A. Polymers for Enhanced Oil Recovery: Fundamentals and Selection Criteria. *Appl. Microbiol. Biotechnol.* **2017**, *101* (11), 4387–4402.

(49) Edomwonyi-Otu, L. C.; Adelakun, D. O. Effect of Heavy Molecular Weight Polymer on Quality of Drinking Water. *Mater. Today Commun.* **2018**, *15*, 337–343.

(50) Azhar, M. R.; Abid, H. R.; Tade, M. O.; Periasamy, V.; Sun, H.; Wang, S. Cascade Applications of Robust MIL-96 Metal Organic Frameworks in Environmental Remediation: Proof of Concept. *Chem. Eng. J.* **2018**, *341*, 262–271.

(51) Loiseau, T.; Lecroq, L.; Volkringer, C.; Marrot, J.; Férey, G.; Haouas, M.; Taulelle, F.; Bourrelly, S.; Llewellyn, P. L.; Latroche, M. MIL-96, a Porous Aluminum Trimesate 3D Structure Constructed from a Hexagonal Network of 18-Membered Rings and M3-Oxo-Centered Trinuclear Units. *J. Am. Chem. Soc.* **2006**, *128* (31), 10223–10230.

https://doi.org/10.1021/ja0621086.

(52) Nandiyanto, A. B. D.; He, X.; Wang, W.-N. Colloid-Assisted Growth of Metal-Organic Framework Nanoparticles. *CrystEngComm* **2019**, *1*, 2268–2272. https://doi.org/10.1039/c9ce00033j.

(53) Benzaqui, M.; Pillai, R. S.; Sabetghadam, A.; Benoit, V.; Normand, P.; Marrot, J.; Menguy, N.; Montero, D.; Shepard, W.; Tissot, A. Revisiting the Aluminum Trimesate-Based MOF (MIL-96): From Structure Determination to the Processing of Mixed Matrix Membranes for CO2 Capture. *Chem. Mater.* **2017**, *29* (24), 10326–10338.

(54) Sindoro, M.; Jee, A. Y.; Granick, S. Shape-Selected Colloidal MOF Crystals for Aqueous Use. *Chem. Commun.* **2013**, *49* (83), 9576–9578. https://doi.org/10.1039/c3cc45935g.

(55) Haouas, M.; Volkringer, C.; Loiseau, T.; Ferey, G.; Taulelle, F. The Extra-Framework Sub-Lattice of the Metal–Organic Framework MIL-110: A Solid-State NMR Investigation. *Chem. Eur. J.* **2009**, *15* (13), 3139–3146.

(56) Haouas, M.; Volkringer, C.; Loiseau, T.; Férey, G.; Taulelle, F. In Situ NMR, Ex Situ XRD and SEM Study of the Hydrothermal Crystallization of Nanoporous Aluminum Trimesates MIL-96, MIL-100, and MIL-110. *Chem. Mater.* **2012**, *24* (13), 2462–2471. https://doi.org/10.1021/cm300439e.

(57) Li, W.; Zhao, H.; Teasdale, P. R.; John, R.; Zhang, S. Synthesis and Characterisation of a Polyacrylamide–Polyacrylic Acid Copolymer Hydrogel for Environmental Analysis of Cu and Cd. *React. Funct. Polym.* **2002**, *52* (1), 31–41.

(58) Morris, W.; Wang, S.; Cho, D.; Auyeung, E.; Li, P.; Farha, O. K.; Mirkin, C. A. Role of Modulators in Controlling the Colloidal Stability and Polydispersity of the UiO-66 Metal–Organic Framework. *ACS Appl. Mater. Interfaces* **2017**, *9* (39), 33413–33418.

(59) Abid, H. R.; Rada, Z. H.; Shang, J.; Wang, S. Synthesis, Characterization, and CO2 Adsorption of Three Metal-Organic Frameworks (MOFs): MIL-53, MIL-96, and Amino-MIL-53. *Polyhedron* **2016**, *120*, 103–111.

(60) Lin, Y.; Kong, C.; Chen, L. Facile Synthesis of Aluminum-Based Metal-Organic Frameworks with Different Morphologies and Structures through an OH--Assisted Method. *Chem. - An Asian J.* **2013**, *8* (8), 1873–1878. https://doi.org/10.1002/asia.201300135.

(61) Gao, X.; Chorover, J. Adsorption of Perfluorooctanoic Acid and Perfluorooctanesulfonic Acid to Iron Oxide Surfaces as Studied by Flow-through ATR-FTIR Spectroscopy. *Environ. Chem.* **2012**, *9* (2), 148–157.

(62) Fu, J. H.; Schlup, J. R. Mid-and Near-infrared Spectroscopic Investigations of Reactions between Phenyl Glycidyl Ether (PGE) and Aromatic Amines. *J. Appl. Polym. Sci.* **1993**, *49* (2), 219–227.

(63) Linder, R.; Seefeld, K.; Vavra, A.; Kleinermanns, K. Gas Phase Infrared Spectra of Nonaromatic Amino Acids. *Chem. Phys. Lett.* **2008**, *453* (1–3), 1–6.

(64) Xue, N.; Wang, L.; Pei, M.; He, Y.; Du, Y.; Guo, W. Preparation and Characterization of Sodium Polyacrylate-Grafted Bentonite and Its Performance Removing Pb 2+ from Aqueous Solutions. *RSC Adv.* **2016**, *6* (101), 98945–98951.

(65) Yu, C.; Liao, R.; Cai, X.; Yu, X. Sodium Polyacrylate Modification Method to Improve the Permeant Performance of Bentonite in Chemical Resistance. *J. Clean. Prod.* **2019**, *213*, 242–250.

(66) Zhang, N.; Yang, X.; Yu, X.; Jia, Y.; Wang, J.; Kong, L.; Jin, Z.; Sun, B.; Luo, T.; Liu, J. Al-1, 3, 5-Benzenetricarboxylic Metal–Organic Frameworks: A Promising Adsorbent for Defluoridation of Water with PH Insensitivity and Low Aluminum Residual. *Chem. Eng. J.* **2014**, *252*, 220–229.

(67) Riahi, K.; Chaabane, S.; Thayer, B. Ben. A Kinetic Modeling Study of Phosphate Adsorption onto Phoenix Dactylifera L. Date Palm Fibers in Batch Mode. *J. Saudi Chem. Soc.* **2017**, *21*, S143–S152.

(68) Kumar, P. S.; Korving, L.; Keesman, K. J.; van Loosdrecht, M. C. M.; Witkamp, G.-J. Effect of Pore Size Distribution and Particle Size of Porous Metal Oxides on Phosphate Adsorption Capacity and Kinetics. *Chem. Eng. J.* **2019**, *358*, 160–169.

(69) Al-Hamairi, A.; AlAmeri, W. Development of a Novel Model to Predict HPAM Viscosity with the Effects of Concentration, Salinity and Divalent Content. *J. Pet. Explor. Prod. Technol.* **2020**, 1–15.

(70) Barton, H. F.; Davis, A. K.; Lee, D. T.; Parsons, G. N. Solvothermal Synthesis of MIL-96 and UiO-66-NH2 on Atomic Layer Deposited Metal Oxide Coatings on Fiber Mats. *J. Vis. Exp.* **2018**, No. 136, e57734. https://doi.org/doi:10.3791/57734.

(71) Deng, S.; Niu, L.; Bei, Y.; Wang, B.; Huang, J.; Yu, G. Adsorption of Perfluorinated Compounds on Aminated Rice Husk Prepared by Atom Transfer Radical Polymerization.

Chemosphere **2013**, *91* (2), 124–130. https://doi.org/10.1016/j.chemosphere.2012.11.015.

(72) Wang, W.; Mi, X.; Shi, H.; Zhang, X.; Zhou, Z.; Li, C.; Zhu, D. Adsorption Behaviour and Mechanism of the PFOS Substitute OBS (Sodium p-Perfluorous Nonenoxybenzene Sulfonate) on Activated Carbon. *R. Soc. Open Sci.* **2019**, *6* (9), 191069.

(73) Zhi, Y.; Liu, J. Surface Modification of Activated Carbon for Enhanced Adsorption of Perfluoroalkyl Acids from Aqueous Solutions. *Chemosphere* **2016**, *144*, 1224–1232. https://doi.org/10.1016/j.chemosphere.2015.09.097.

(74) Zhao, H.; Gao, J.; Zhao, G.; Fan, J.; Wang, Y.; Wang, Y. Fabrication of Novel SnO2-Sb/Carbon Aerogel Electrode for Ultrasonic Electrochemical Oxidation of Perfluorooctanoate with High Catalytic Efficiency. *Appl. Catal. B Environ.* **2013**, *136–137*, 278–286. https://doi.org/10.1016/j.apcatb.2013.02.013.